Composites Science and Technology 72 (2012) 314–319

Contents lists available at SciVerse ScienceDirect

Composites Science and Technology

journal homepage: www.elsevier.com/locate/compscitech

Gradient of nanomechanical properties in the interphase of cellulose nanocrystal composites

Anahita Pakzad [a], John Simonsen [b], Reza S. Yassar [a,*]

[a] Mechanical Engineering – Engineering Mechanics, Michigan Technological University, Houghton, MI 49931, USA
[b] College of Forestry, Oregon State University, Corvallis, OR 97331, USA

ARTICLE INFO

Article history:
Received 8 June 2011
Received in revised form 25 October 2011
Accepted 15 November 2011
Available online 25 November 2011

Keywords:
A. Nano composites
B. Interphase
B. Mechanical properties

ABSTRACT

The nanoscale transitional zone between a nanofiber and surrounding matrix (interphase) defines the ultimate mechanical characteristics in nanocomposite systems. In spite of this importance, one can hardly find quantitative data on the mechanical properties of this transitional zone in the cellulose–nanofiber composites. In addition, most of the theoretical models to predict the mechanical properties of interphase are developed with the assumption that this transitional zone is independent of the nanofiber size. In the current study, we show that the mechanical properties of interphase in cellulose nanocrystal (CNC) composites can be quantitatively characterized and the correlation with the size of CNCs can be mapped. The peak force tapping mode in atomic force microscope (AFM) was used to characterize deformation, adhesion, and modulus gradient of the interphase region in poly(vinyl alcohol) (PVA)–poly (acrylic acid) (PAA)–cellulose nanocrystal (CNC) composites. In comparison to the polymer matrix, the adhesion force of CNC was lower. The average elastic modulus in the interphase varied from 12.8 GPa at the interface of CNC to 9.9 GPa in PVA–PAA matrix. It was observed that the existence of PAA increased the gradient of mechanical and adhesion properties of the interphase zone. This occurs due to the variation in the ester linkage density from the CNC interface to the polymer matrix. Finally, it is shown that interphase thickness is higher for CNCs with larger diameter.

1. Introduction

Poly(vinyl alcohol) (PVA) is a water soluble polymer. It is largely produced and has been extensively used as a membrane since it is a good barrier against oxygen and aromas and is resistant to permeation of solvents and oils. PVA barrier membranes do not have sufficient mechanical properties [1–3] and have poor stability at high moisture contents [4]. This happens because water molecules swell PVA and degrade its barrier functionality. Paralikar et al. [5] have shown that the addition of 10 wt.% cellulose nanocrystals (CNCs) to PVA and cross linking it using 10 wt.% poly(acrylic acid) (PAA) improves the overall mechanical properties of the composite. They showed that PAA acted as a cross-link agent and an ester linkage was formed between the carboxyl groups in PAA and hydroxyl groups in CNC and PVA, which resulted in a highly networked structure with improved properties.

One of the drawbacks of using CNCs is their high tendency to agglomerate due to the large number of hydroxyl groups on their surface (highly polar and hydrophilic). This makes dispersion of these crystals very difficult in polymer matrices, especially those that are non-polar or hydrophobic. In this case the properties of interfacial zone or interphase can play a major role in overall properties of the cellulose nanocrystal composite materials. This interphase represents a heterogeneous transition zone, which separates the bulk polymer from the CNC reinforcement. In general the size of interphase can vary between nanometers to micrometers [6]. Interphase is formed due to local physical or chemical changes (cross linking, immobilization, crystallization of polymer, interdiffusion of atoms or molecules, etc.) that are dictated by the surface of the reinforcement. In the literature one can find several approaches and characterization techniques to identify the interphase properties. These include nuclear magnetic resonance spectroscopy (NMR) [7], Fourier transform infrared spectroscopy (FTIR) [8], ion scattering spectroscopy (ISS) and secondary ion mass spectroscopy (SIMS) [9], X-ray photoelectron spectroscopy (XPS) [10], stereoscopic displacement analysis [11], and nanoindentation [11,12].

One of the limitations of the above techniques is their spatial resolution. Therefore, scanning probe microscopy (SPM) techniques, and particularly atomic force microscopy (AFM) with resolution less than 0.1 Å, can fill this gap. First attempts for characterization of the interphase using AFM were based on the contact and force modulation modes [13]. Force modulation

* Corresponding author.
E-mail address: reza@mtu.edu (R.S. Yassar).

0266-3538/$ - see front matter © 2011 Elsevier Ltd. All rights reserved.
doi:10.1016/j.compscitech.2011.11.020

involves modulating the tip-sample interaction force as the AFM tip moves across the sample surface in contact mode. AFM has also been used as a nanoindenter [14,15] to characterize the mechanics of the interphase region. For this purpose either an indenter probe is attached to the end of a capacitive load sensor or a stainless steel cantilever with a diamond tip is used. Another approach for characterization of the interphase in AFM is based on phase imaging, which is similar to force modulation techniques but is performed in tapping mode [16]. The phase image is generated simultaneously with the topographic image as a result of changes in the phase angle of the cantilever due to change in topography, tip-sample interaction, and experimental conditions [17]. The sine phase image contains only the qualitative data; it does not provide a basis to accurately measure the properties of the interphase region.

To the authors' knowledge, no reports have documented the quantitative mechanical properties of the interphase in cellulose-composite systems. Here, the purpose was to study the mechanical properties of the interphase region in CNC-based nanocomposites. Peak force tapping mode (PF–TM) was used for obtaining quantitative nanomechanical (QNM) maps of the interphase in PVA–PAA–CNC composite films. This work demonstrates, for the first time, the direct measurements of the gradient in adhesion and elastic modulus in CNC-based nanocomposites at the nanoscale interphase. Lastly, the effect of CNC size was investigated on the interphase thickness.

2. Materials and methods

Materials studied in this work were prepared as described elsewhere [5]. Briefly, CNCs were prepared by partial acid hydrolysis of cotton (Whatman #1 filter paper, Clifton, NJ). Filter paper was ground and stirred with 65% H_2SO_4 (v/v) for 50 min, at 45 °C. The cotton-to-acid ratio was 1:10 g ml^{-1}. After the mixture was centrifuged five times, it was subjected to ultrasonication (Branson Sonifier, Danbury, CT) for 15 min, in order to break agglomerations and evenly disperse CNCs in water. To remove the remaining salts, ultra filtration was done until the conductivity was <10 μS cm^{-1}, (Ultrasette tangential flow UF device, pore size = 50 nm, Pall Corp., Ann Harbor, MI). Finally, an aqueous suspension of 1% CNC was obtained by concentrating the dispersion of CNCs in a Rotavaporizer R110 (Buchi, Flawil, Switzerland). Poly(vinyl alcohol), (99 + % hydrolyzed, M_w = 89,000–98,000 g mol^{-1}) was obtained from Sigma–Aldrich Inc. (St Louis, MO). Poly(acrylic acid), (M_w = 2000 g mol^{-1}) was obtained from Aldrich Chemical Company Inc. (Milwaukee, WI).

Solutions of PVA and PAA were prepared by dissolving their powder in DI water and stirring in an oil bath for 30 min, at 85 °C. Calculated volume of component solutions and CNC dispersions (80 wt.% PVA, 10 wt.% PAA, 10 wt.% CNC) were then blended and sonicated for 25 min to disperse any remaining aggregates. Then mixtures were casted in a flat-bottom plastic dish and air dried for 48 h. Finally the samples were heat treated at 170 °C for 45 min. A sample of 80 wt.% PVA and 15 wt.% CNC was also prepared to investigate the effect of existence of PAA on the properties of the interphase.

3. QNM analysis: PF–TM in AFM

In peak force tapping mode (PF–TM) technique, using the main Z piezo element, the vertical motion of the cantilever is oscillated below its resonant frequency. For each individual tap, nanoscale material property and peak force is collected by collecting one force curve at each pixel (Fig. 1) [18]. Each force-separation curve is then analyzed to generate material property maps with the same resolution as the height image. PF–TM relies on the maximum

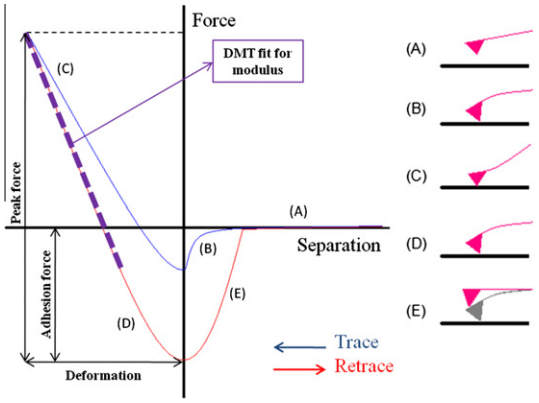

Fig. 1. *Left:* Schematic of force-separation curve obtained during the AFM tip tapping on the samples surface. The blue curve (trace) represents the loading portion and the red curve (retrace) indicates the unloading part. Part of the unloading curve (bold dashed line) is used to calculate the Derjaguin–Muller–Toropov (DMT) elastic modulus [15]. The minimum force in the retrace curve is used for mapping the adhesion properties. Also, the peak force value is used for peak force imaging in AFM. *Right:* tip-sample interactions during each tap. At (A) there is little or no force on the tip. As the piezo expands (separation decreases), the tip is pulled down (B) by attractive forces such as van der Waals, capillary or electrostatic, until it touches the surface (separation = 0). Then the tip is pushed into the sample until the set point for the peak force is reached (C). The piezo then starts to pull up the tip and the force keeps decreasing (D) to a minimum value, where the tip comes off the surface. After this point forces affecting the tip keep decreasing as separation increases (E) and piezo returns to its initial position. (For interpretation of the references to color in this figure legend, the reader is referred to the web version of this article.)

interaction force between the tip and the sample (peak force) as the feedback signal. By controlling the maximum force, smaller deformation is formed on the surface (<3 nm), which increases the imaging resolution and decreases the tip wear.

During data acquisition the deflection of the cantilever (Δ in V) and the position of the piezo (z in nm) are recorded at each tap (or pixel). In order to convert this data to force in nN versus separation in nm, the deflection sensitivity of the cantilever should be measured. This is the distance that the cantilever is really deflected for a measured change in the photo-detector voltage (nm V^{-1}). Deflection sensitivity depends on the cantilever type and the laser path from the back of the cantilever to the detector. Deflection sensitivity converts the units of Δ to nm. Force (F) can then be easily calculated in nN, by multiplying the deflection of the cantilever by its spring constant, k($F = k\Delta$). Separation is by definition the negative value of deformation and is calculated by adding the vertical piezo position (z) to the cantilever deflection. From the force separation curve for each pixel, peak force, adhesion force, deformation, and elastic modulus values are sent to separate imaging channels. QNM imaging continues at usual imaging speed and material property maps are generated simultaneously with the height image.

On each force curve (Fig. 1), peak force is the maximum force value and it is used as the feedback signal in PF–TM. Adhesion force is the minimum force value, which is affected by the interaction between the tip and the sample and increases with the tip end radius. Deformation is the difference of the separation from force equal to zero to the peak force. Lastly, the elastic modulus is calculated by fitting the Derjaguin–Muller–Toropov (DMT) model [19] to the initial section of the retrace curve (bold dashed line in Fig. 1):

$$F = \frac{4}{3}E^*\sqrt{Rd^3} + F_{adh} \quad (1)$$

where F is the force on the tip, R is the tip radius, d is the separation, F_{adh} is the adhesion force and E^* is the reduced elastic modulus. Knowing the Poisson's ratio of the sample (υ_s) and the tip (υ_{tip})

and assuming infinite elastic modulus for the tip (E_{tip}), the elastic modulus for the sample (E_s) can be calculated:

$$E^* = \left(\frac{1-\nu_s^2}{E_s} + \frac{1-\nu_{tip}^2}{E_{tip}}\right)^{-1} \quad (2)$$

4. AFM measurements

Dimension© Icon© AFM was used for the force probing in this work. Silicon AFM probes with nominal spring constant of 20–80 N m^{-1} and tip radius of 5–12 nm were used. The deflection sensitivity of the cantilever was measured by acquiring a force curve on a hard sapphire surface. This was repeated at least at five positions to make sure the value was consistent (104.75 N m^{-1}). The spring constant was acquired to be 24 N m^{-1}, using the Sedar's method [20]. It is worth mentioning that such high spring constant cantilever was selected in order to reduce the amount of cantilever bending during AFM data acquisition.

The tip radius was measured using the relative method. This briefly included scanning a standard sample (Poly Styrene) with a known elastic modulus, and changing the tip radius in Nanoscope software until the expected value (2.7 GPa) was obtained in the elastic modulus channel. Tip radius for 2 nm deformation was equal to 5 nm. Finally the Poisson's ratio value of 0.3 was used for three phases in the composite. These settings were kept constant for all the subsequent measurements.

The AFM images consisted of 512 × 512 pixels. Scanning rate was changed according to the scan size and was <1 Hz at all times. The peak force was set such that the resultant average deformation in each scan line was not more than 3 nm. Other scanning parameters such as integral and proportional gains were automatically set by the Nanoscope software.

5. Elastic modulus and adhesion at the interphase

Fig. 2 depicts the height and adhesion images acquired on the composite samples. These large scans (50 × 50 μm^2) were acquired to find CNCs through the polymer matrix. Due to the fact that CNCs are embedded in the matrix, the height image (Fig. 2a) is not able to detect the presence of CNCs. In most cases CNCs (shown by yellow arrows) had almost the same height as the surrounding polymer; therefore not much image contrast appeared in the height map. On the other hand, the difference in adhesion properties of CNCs and polymer matrix provided apparent contrast in the adhesion maps and made it possible to distinguish CNCs from neighboring polymer (Fig. 2b). In general, throughout the sample, the adhesion of the tip to the polymer matrix (36 ± 7.2 nN) was higher compared to its adhesion to CNCs (25.6 ± 4.3 nN). The difference can be explained by the repulsive forces that can occur between the negative surface charges on the CNC surface (after sulfuric acid hydrolysis [21]) and the thin oxide layer on the AFM tip.

Fig. 3a shows the three-dimensional (3D) height image of a CNC aggregate, where the width gradually changes from one end to another. The corresponding adhesion and elastic modulus maps are shown in Fig. 3b and c, respectively. The average variation of mechanical properties in the region, identified by the red box, can be seen in Fig. 3d. The blue and orange curves in Fig. 3d represent the adhesion and elastic modulus profiles, respectively. According to the elastic modulus profile, the detected mechanical properties are higher in the locations where CNCs exist. In contrast, the adhesion properties are lower in the locations of CNCs. This is consistent with the observation made in Fig. 2b. The scattering of the data observed on the profiles in Fig. 3d can be due to the influence of surface roughness and small indentation depth made at each tap.

As shown in Fig. 3d, the elastic modulus of CNC (12.8 ± 3.1 GPa) was found to be higher than PVA–PAA matrix (9.9 ± 1.1 GPa). One should note that the CNC elastic constants reported here are the average transverse moduli (E_T) and are close to the previously reported data [22–24]. Tashiro and Kobayashi [24] calculated the elastic modulus of CNC in two orthogonal directions perpendicular to the CNC axis ($T1$ and $T2$) equal to E_{T1} = 51 and E_{T2} = 57 GPa. Lahiji et al. [22] used nanoindentation in AFM and measured the transverse elastic modulus of cotton CNCs varying between 18 and 50 GPa at 1% relative humidity. Nakamae et al. [23] used an X-ray diffraction technique and estimated the theoretical transverse elastic modulus of PVA to be E_T = 6–9 GPa.

Next, the variation in matrix properties as a function of distance from the surface of CNC was studied. As seen in Fig. 3, the elastic modulus gradually changed from ~12.8 GPa at the CNC interface to ~9.9 GPa at PVA–PAA interface. The distance over which the properties changed is called 'interphase' hereafter. The gradual change in nanomechanical properties of the interphase can be explained by gradient distribution of ester linkages (cross linking density) from the CNC interface to the polymer matrix. Fig. 4a shows the schematic of a CNC embedded in a pure PVA matrix. Here, no PAA chains exist in the composite and only PAA molecules surround CNC via hydrogen bonds with its surface. Fig. 4b and c show the schematics of a cellulose nanocrystal embedded in

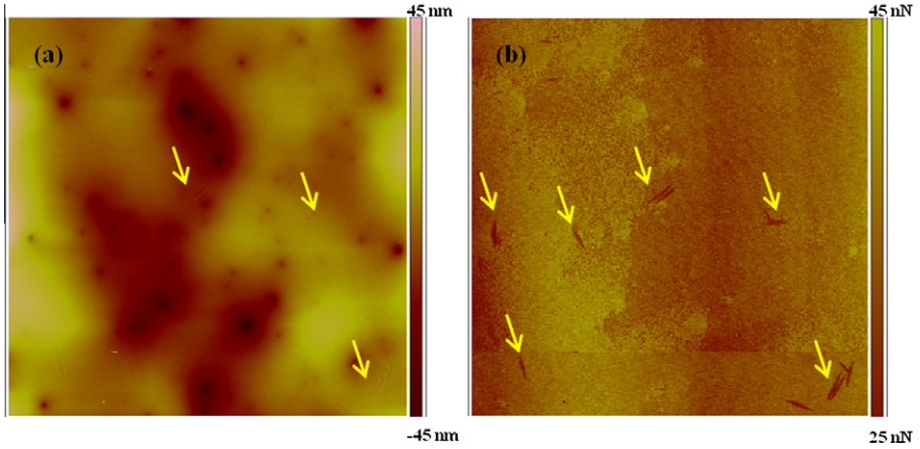

Fig. 2. (a) Height and (b) adhesion maps of a 50 × 50 μm^2 region on a PVA 80–CNC 10–PAA 10 sample. The arrows point to CNCs embedded in the polymer matrix. The presence of CNCs is easily distinguishable from the adhesion image.

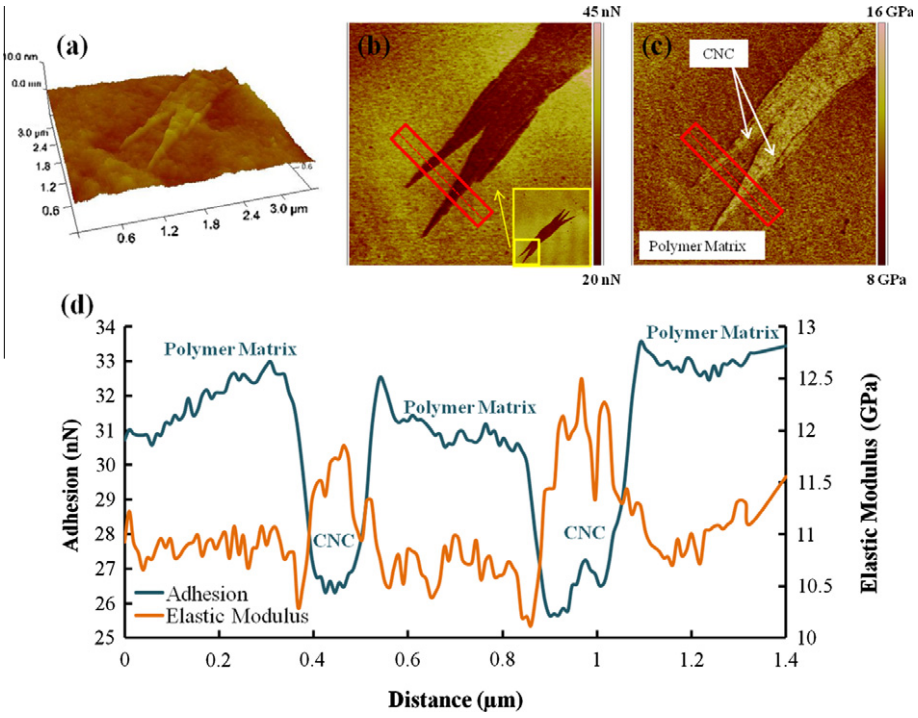

Fig. 3. (a) 3D height, (b) adhesion, and (c) elastic modulus maps (3.5 × 3.5 μm^2). Inset in (b) shows the scanning area (PVA 80–CNC 10–PAA 10). (d) The average adhesion and elastic modulus profiles of the area in the red boxes in (b) and (c). Polymer matrix and CNC regions are marked on the profile. Interphase region is the distance that adhesion and modulus profiles are overlapped.

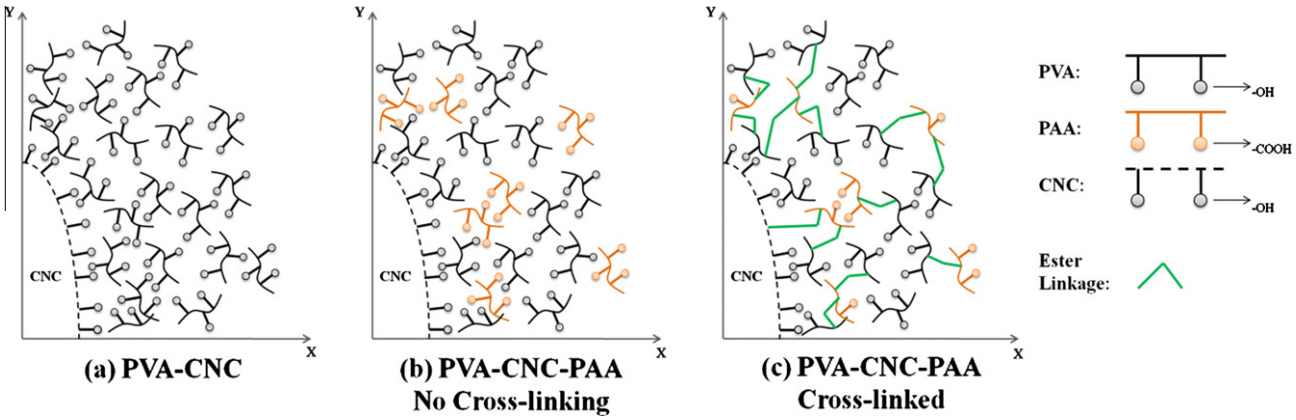

Fig. 4. Structural models of PVA membranes containing (a) no PAA, (b) PAA and before cross-linking, and (c) PAA and after cross linking. In PVA–CNC membrane, only hydrogen bonds between CNC and PVA exist at the interphase. In the PVA–CNC–PAA case (before cross-linking), PVA molecules form hydrogen bonds with hydroxyl groups on the CNC surface. Some PAA molecules also exist in the vicinity of CNC. After cross-linking, ester bonds form and the population of these bonds decreases as the distance from CNC surface increases (figure is not to scale).

PVA–PAA polymer matrix before and after the cross-linking process. In Fig. 4b (before ester links are formed), there is no covalent bond between PVA, PAA, and CNC. PVA molecules surround CNC and form hydrogen bonds with cellulose crystal as well as each other. On the other hand, not many PAA molecules are present close to the CNC surface. The surface energy between CNC and PVA is lower than the surface energy at CNC–PAA interface and this can be explained by great likelihood of formation of hydrogen bonds between CNC and PVA as opposed to CNC and PAA. Hyder et al. [25] have reported that measuring the contact angle for pure PVA films is not possible because water swells the polymer in less than a minute. This shows the hydrophilic nature of PVA and, in other words, its high tendency to form hydrogen bonds. PAA is not very hydrophilic, and does not form hydrogen bonds. For this same reason polar components are usually added to PAA to act as hydrogen bond accepters and to improve the PAA's adhesive properties [26]. After the composite is heated, ester links are formed between PVA–PAA, PVA–PAA–CNC or CNC–PAA (Fig. 4c). Here, due to esterification, the number of hydroxyl groups on CNC surface is less than prior to cross-linking. Thus, hydrogen bonding still exists but is less between CNC and PVA. Formation of ester linkages results in the improvement of mechanical property and thermal stability of PVA membranes [5]. Likewise, existence and density of these links in the vicinity of CNC can affect the properties of the interphase.

In order to investigate the effect of ester links that form due to the existence of PAA, the rate of change in adhesion at the interphase was calculated for two composite systems; one with PAA and cross linked (PVA 80–CNC 10–PAA 10, rectangular symbols in Fig. 5) and one without PAA (PVA 85–CNC 15–PAA 0, triangle

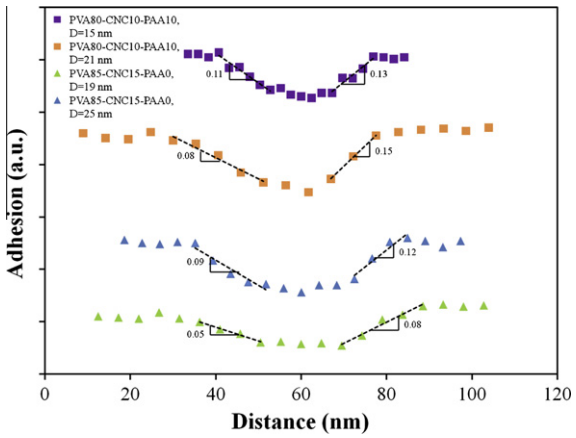

Fig. 5. Average adhesion profiles (arbitrary unit, a.u.) in PVA 80–CNC 10–PAA 0 (square) and PVA 85–CNC 15–PAA 0 (triangle) composites. Dashed lines were used to measure the rate of change in adhesion at the interphase (nN nm^{-1}).

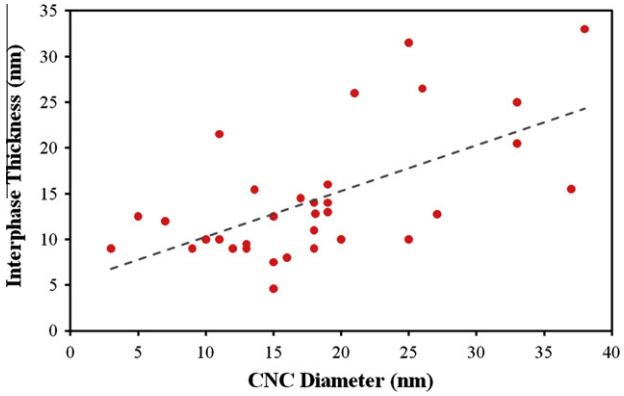

Fig. 7. Change in interphase thickness with CNC diameter. Red circles show average interphase thickness of the CNCs. The trend line (dashed gray line) shows an increasing trend in the interphase thickness with the CNC diameter. (For interpretation of the references to colour in this figure legend, the reader is referred to the web version of this article.)

symbols in Fig. 5). For this purpose, the average adhesion profiles were acquired at CNC sites in each sample. Slopes of these curves were calculated at the interphase regions (dashed lines on Fig. 5). In order to rule out the dependency on CNC size, care was taken to select CNCs with similar diameters. It was found that the rate of change in adhesion at the interphase was 0.08 ± 0.03 nN nm^{-1} in PVA 85–CNC 15–PAA 0, while this rate was 0.12 ± 0.02 nN nm^{-1} in PVA 80–CNC 10–PAA 10 samples. This is equivalent to ~33% difference in the rate of change in adhesion in these two samples. This difference confirms that the existence of PAA has increased the gradient of mechanical properties of the interphase.

Similar to PVA 80–CNC 10–PAA 10 membrane, the existence of gradient in mechanical properties in PVA 85–CNC 15–PAA 0 sample is expected. It was observed that the mechanical properties decrease from the CNC surface to the PVA matrix. This can be explained by the gradient in hydrogen bonding from the CNC surface towards the polymer matrix. As shown in Fig. 4a, at the surface of CNC, CNC–CNC, PVA–PVA, and PVA–CNC hydrogen bonds coexist. The number of PVA–CNC hydrogen bonds decreases from the surface of CNC into the polymer matrix, where only PVA–PVA bonds are present (Fig. 4a). The number and nature of these hydrogen bonds have substantial effect on the mechanical properties in such molecular materials [23,24,27,28].

6. Interphase thickness and CNC diameter

The ability to measure the thickness of interphase in nanocomposites allows one to study the relationship between the interphase size and the size of the reinforcement. Here, in order to study size dependency of interphase is on the CNC size, the interphase thickness was measured on both sides for various CNCs in the composite system. Fig. 6a depicts an individual CNC with diameter of ~9 nm, measured from the adhesion image (Fig. 6b). The adhesion map shows that the mechanical properties of the CNC are fairly uniform along its axial direction. The thickness of interphase was between 11 and 13 nm on either sides of this crystal (Fig. 6c). Using such profiles and the corresponding adhesion maps, the CNC diameters and interphase thickness on either sides of CNCs were recorded. The average interphase thickness was calculated using the size of the interphase on both sides.

Fig. 7 depicts the variation in the average interphase thickness as a function of CNC size. As seen, the interphase thickness increased with the increase of CNC diameter. Depending on the size of the CNC, the thickness of the interphase varied between 4 and 35 nm. For instance, taking two CNCs with similar aspect ratios (length/diameter = 50) and different diameters of 10 and 30 nm, the surface area, for the CNC with diameter equal to 30 nm, (142,713 nm^2) is ~9 times larger than that of the smaller CNC. This larger surface area can give rise to a thicker interphase [29,30].

To the authors' knowledge, this is the first nanoscale experimental effort to characterize the size of interphase in CNC-composite systems. Our data can be important to those interested in developing accurate models of interface in nanocomposite systems [31–33]. Brown et al. [31] studied the effect of nanoparticle diameter on the thickness of interphase by molecular dynamics. They found that the thickness of interphase remained constant independent of the inclusion size and volume fraction of reinforcement. In another work, Li et al. [33] utilized a hierarchical multi-interphase

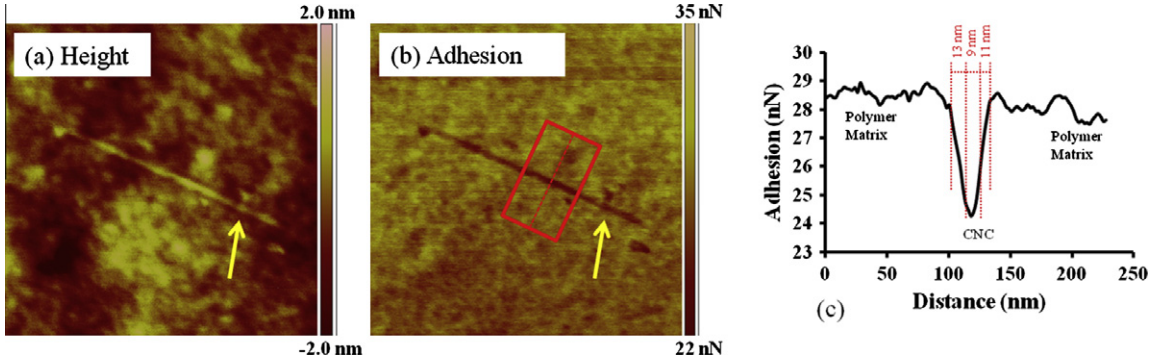

Fig. 6. (a) Height and (b) adhesion maps with size of 1 × 1 μm^2 showing a single CNC (marked by yellow arrows). (c) Average adhesion profile of the area shown by red rectangle in adhesion map in (b). Using this profile, CNC diameter (9 nm) and average thickness of the interphase were measured. (For interpretation of the references to colour in this figure legend, the reader is referred to the web version of this article.)

model and showed that the volume fraction of the interphase is size-independent. They concluded that the effect of interphase thickness on the reinforcing efficiency of nanomaterials vanishes as length is increased above 40 nm. The present investigation shows that the thickness of the interphase is not constant and should be taken into account in future theoretical frameworks for the interphase consideration and particularly in the CNC-polymer composite systems.

7. Conclusions

Nanomechanical properties of the interphase (the zone between CNC surface and polymer matrix) were quantitatively characterized in poly(vinyl alcohol)–poly(acrylic acid)-cellulose nanocrystal composites using peak force tapping mode in AFM. As opposed to topography images, nanomechanical and adhesion maps enabled the detection of CNCs embedded in the PVA–PAA polymer matrix. The interphase in the composites containing PAA exhibited a higher gradient in adhesive and mechanical properties in comparison to the samples with no PAA. From the polymer matrix to the CNC surface, the average elastic modulus increased from 9.9 to 12.8 GPa, and the adhesion to the AFM tip decreased from 36 to 25.6 nN, respectively. The observation of higher gradient in properties of the composites with PAA was related to the increase in the density of ester linkages from the polymer matrix to the CNC interface. It was also shown that the interphase thickness depended on the CNC size. Because larger CNCs have higher surface area, the influence of CNC penetrates deeper in the polymer and results in higher interphase thickness.

Acknowledgements

The authors acknowledge the National Science Foundation (NSF) for the Grants Nos. 0820884 and 11000806/1100572 from Division of Materials Research (DMR). Also, thanks to Dr. M.C. Frost for constructive discussions on the data.

References

[1] Cadek M, Hedicke K, Blau WJ. Appl Phys Lett 2002;81:5123–5.
[2] Liu L, Barber AH, Nuriel S, Wanger HD. Adv Funct Mater 2005;15:975–80.
[3] Cheng Q, Wang S, Rials TG, Lee S. Cellulose 2007;14:593–602.
[4] Roohani M, Habibi Y, Belgacem NM, Ebrahim G, Naghi Karimi A, Dufresne A. Eur Polymer J 2008;44:2489–98.
[5] Paralikar SA, Simonsen J, Lombardi J. J Membr Sci 2008;320:248–58.
[6] Drzal LT. Adv Polym Sci 1986;75:1–32.
[7] Droste DH, Dibenedetto AT, Stejskal EO. J Polym Sci 1971;9:187–9.
[8] Ishida H, Koenig JL. J Colloid Interf Sci 1978;64:555–65.
[9] Dibenedetto AT, Scola DA. J Colloid Interf Sci 1978;64:480–500.
[10] Thomason JL, Dwight DW. Composites Part A 1999;30:1401–13.
[11] Williams JG, Donnellan ME, James MR, Morris WL. Mater Sci Eng 1990;126:305–12.
[12] Hodzic A, Stachurski ZH, Kim JK. Polymer 2000;41:6895–905.
[13] Mai K, Mader E, Muhle M. Composites Part A 1998;29:1111–9.
[14] VanLandingham MR, McKnight SH, Palmese GR, Elings JR, Huang X, Bogetti TA, et al. J Adhes 1997;64:31–59.
[15] Winter RM, Houston JE. Proc Soc Exp Mech Spring Conf Exp Appl Mech 1998:355–8.
[16] Downing TD, Kumar R, Cross WM, Kjerengtroen L, Kellar JJ. J Adhes Sci Technol 2000;14:1801–12.
[17] Raghavan D, Gu X, Nguyen T, VanLandingham M, Karim A. Macromolecules 2000;33:2573–83.
[18] Pittenger B, Erina N, Chanmin S. Bruker application note. Quantitative mechanical mapping at nanoscale with peak force QNM; 2009.
[19] Derjaguin BV, Muller VM, Toropov Y. J Colloidal Interface Sci 1975;53:314–26.
[20] Ohler B. Bruker application note. Practical advice on determination of cantilever spring constants; 2009.
[21] Habibi Y, Lucia LA, Rojas OJ. Chem Rev 2010;110:3479–500.
[22] Lahiji RR, Xu X, Reifenberger R, Roman A, Rudie A, Moon RJ. Langmuir 2010;26:4480–8.
[23] Nakamae K, Nishino T, Hata K, Matumoto T. Kobunshi Ronbunshu 1986;42:881–8.
[24] Tashiro K, Kobayashi M. Polymer 1991;32:1516–26.
[25] Hyder MN, Huang RYM, Chen P. J Membr Sci 2006;283:281–90.
[26] Shojaie A, Xiaoling Li. J Controlled Release 1997;47:151–61.
[27] Tashiro K, Tadokoro H. Macromolecules 1981;14:781–5.
[28] Peijs T, van Vught RJM, Govaert LE. Composites 1995;26:83–90.
[29] Long D, Lequeux F. Eur Phys J E 2001;4:371–87.
[30] Liu H, Catherin Brinson L. Compos Sci Technol 2008;68:1502–12.
[31] Brown D, Marcadon V, Mele P, Alberola ND. Macromolecules 2008;41:1499–511.
[32] Jancar J, Douglas JF, Starr FW, Kumar SK, Gassagnau P, Lesser AJ, et al. Polymer 2010;51:3321–43.
[33] Li Y, Waas AM, Arruda EM. J Mech Phys Solids 2011;59:43–63.